7

Hybrid Polyfluorene-Based Optoelectronic Devices

Sylvain G. Cloutier
École de Technologie Supérieure
Canada

1. Introduction

It is now well established that controlled delocalization in π-conjugated chains can lead to unique optoelectronic properties in polymer materials (MacDiarmid, 2001). While still being in a relatively early developmental stage, conjugated-polymer systems with a myriad of optoelectronic properties can now be synthesized at relatively low costs. Albeit a very promising technology, there remains some key challenges to address before efficiently integrating these conjugated-polymer systems into large scale applications including displays, biomedical imaging & sensing, lab-on-a-chip, solid-state lighting and photovoltaic devices and architectures (Arias et al., 2001; Moons, 2002; Morteani et al., 2003).

Pending material issues still limit the functionality and the overall performances of these emerging material systems, while photo-chemical degradation can severely restrict their lifetimes. Since the main photo-chemical degradation process is usually a photo-oxidation reaction that truncates the conjugation length of the polymer chain to reduce the π-electron delocalization, this undesireable process can be significantly suppressed by simply permeating the structure with a transparent dielectric coating. Using such coating technologies, lifetimes of 20 years have now been demonstrated for commercial polymer-based photovoltaic devices and displays.

In the last few years, the hybrid integration of semiconductor nanocrystals within conjugated polymer host systems has grown into a very active research area as it provides a new pathway of (1) improving the conjugated polymers' optoelectronic properties and/or (2) providing added functionality to the conjugated polymer-based structures.

This chapter will present a general overview of hybrid polymer-nanocrystal material systems and their application as low-cost optoelectronic devices. Using a device-engineering perspective, we will focus our attention on the synthesis & processing, structural and optoelectronic properties of polyfluorene-based systems interfaced with lead-sulfosalt (PbS) semiconductor nanocrystals grown by hot-colloidal methods. Using this specific hybrid material system as our case study, we will begin by providing a general understanding of pure polymer-based type-II heterostructures and their limitations. Then, we will demonstrate how the incorporation of lead-chalcogenide quantum dots can be used to (1) add new functionality and (2) improve the performances of those all polyfluorene-based optoelectronic devices. Most importantly, we will also see that the hybrid integration of

conjugated polymers and colloidal quantum dots also raises many important fundamental questions and crucial technical challenges to address before achieving low-cost hybrid optoelectronic devices with superior performances.

In the long-term, we strongly believe this emerging class of hybrid polymer-based heterostructures will potentially transform the field of opto-electronics by providing low-cost and high-performance semiconductor-based nanocomposite materials and devices for applications such as light sources, biomedical & lab-on-a-chip devices, flexible and/or high-performance optoelectronics platforms and photovoltaics.

2. Polyfluorene-based type-II heterostructures

Compared to more commonly-used π-conjugated polymer families such as the polyphenylenes (PPPs and PPVs), polythoiphenes (PTs), polypyrroles (PPYs) and polyanilines (PANIs), polyfluorenes tend to be easier to process and less sensitive to photo-chemical degradation while still offering very decent optoelectronic properties. This combination of facile processing and durability makes polyfluorenes an ideal case-study platform.

In particular, relatively efficient polymer light-emitting structures for the visible have been previously realized using polyfluorene-based type-II heterostructures fabricated using poly(9,9-dioctylfluorene-co-N-(4-butylphenyl)diphenylamine (or **TFB**) as the hole-transporting material and poly(9,9′-dioctylfluorene-co-benzothiadiazole (or **F8BT**) as the electron-transporting polymer (Moons, 2002).

Meanwhile, decent photovoltaic structures have also been realized using similar polyfluorene-based type-II heterostructures. However, the best performances reported so far for polyfluorene-based photovoltaics were also using F8BT as the electron-transporting polymer but replacing the hole-transporting TFB with poly (9,9′-dioctylfluorene-*co*-bis-*N,N*′-(4-butylphenyl)-bis-*N,N*′-phenyl-1,4-phenylenediamine)   (or **PFB**) (McNeill et al., 2009).

Finally, it is important to mention that while hole-transporting π-conjugated polymers with conductivities over 1000 $\Omega^{-1}cm^{-1}$ have been reported, decent electron-transporting polymers are much more difficult to come by. As such, the electron-transporting material often limits the overall performances of polymer-based optoelectronic devices (Moons, 2002).

2.1 Blended all polyfluorene-based type-II heterostructures for light-emitting and photovoltaic device architectures

TFB-F8BT system provides a great material platform to understand the basic principles associated with conjugated polymer-based optoelectronic devices. For the typical light-emitting diode (LED) configuration shown in Figure 1(a), the hole-transporting TFB (labeled HTL) and electron-transporting F8BT (labeled ETL) are used to provide a type-II heterostructure. In this configuration, holes are injected from the transparent ITO anode while electrons are injected from the Aluminum cathode. To facilitate carrier injection and reduce exciton quenching at the electrode-polymer interface, optional hole- and electron-injection layers can be introduced in such device architectures. Here, a thin layer of poly(ethylenedioxythiophene):polystyrenesulphonate (or **PEDOT:PSS**) can be used to

facilitate the hole injection and improve the structural quality of the TFB film by alleviating the surface roughness of the indium-tin oxide (ITO) substrate. In contrast, a thin layer of low work-function metal such as Calcium can be used to facilitate the electron-injection on the other side of the junction. In such a case, the Aluminum contact remains necessary to prevent oxidation of the low work-function metal. In this system, injected carriers bind into an exciton at the TFB-F8BT interface. Due to the band alignment, this exciton is much more likely to migrate to the electron-transporting F8BT until it recombines radiatively and generates the emission.
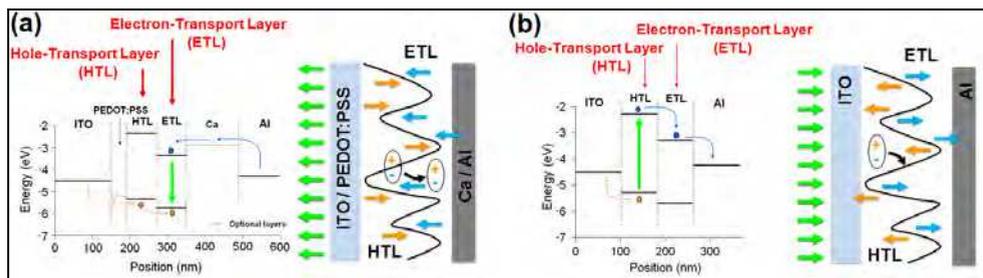

Fig. 1. Energy diagrams and schematics of TFB-F8BT polyfluorene-based type-II heterostructures. (a) For use as visible light-emitting diode. (b) For use as a photodetector or solar cell device structure.

In contrast, Figure 1(b) illustrates how a similar heterostructure can be used as a photovoltaic device. There, the exciton is photo-generated in the hole-transporting TFB and dissociates upon meeting the energy barrier at the TFB-F8BT interface to allow carrier extraction. Of course, this structure does not require the PEDOT:PSS and Ca layers previously used to facilitate carrier injection.

Due to the very low mobilities in conjugated polymers compared with conventional semiconductors, it is clear that the bulk of these devices' optoelectronic properties stem from the interface between the hole- and electron-transporting polymers. In the case of polymer-based LED structures, the exciton will usually recombine within tens of nanometers from the ETL-HTL interface. Meanwhile, any exciton generated more than tens of nanometers from the ETL-HTL interface in photovoltaic device structures will recombine radiatively before reaching the surface and those carriers will be lost. To enable an easy processing, these all polyfluorene-based type-II heterostructures are usually formed using a **blended** precursor solution containing both polymers dissolved in a given solvent. When this blend is deposited on the ITO substrate by spin- or dip-coating, phase-separation occurs as the solvent evaporates. This leads to the formation of HTL-rich and ETL-rich domains such as shown in Figure 2 (Moons, 2002).

2.2 The importance of the domain sizes and the crystalline phase in polyfluorene-based thin-film structures

Based on the previous discussion, we now understand that the optoelectronic properties of those conjugated polymer-based heterostructures will depend largely on the interface between the hole-transporting and electron-transporting polymers. As such, an intuitive
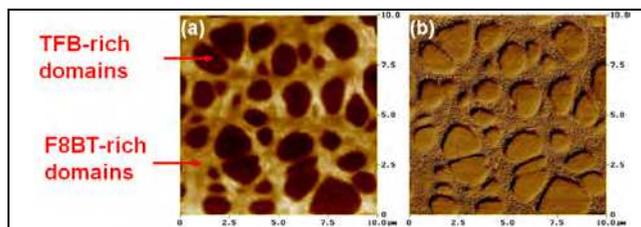
Fig. 2. Example of a large domain structure in a polyfluorene-based type-II heterostructures using xylene-based precursor measured using AFM. Adapted from (Moons, 2002) with permission.

way to controllably alter the optoelectronic properties of those structures would be to control the domain size. One relatively simple way of doing this is by changing the solvent used in the precursor solutions. Since the domains form by phase-separation, faster evaporations rates (using solvents such as chloroform, acetone or hexane) will generally yield significantly smaller domains compared with lower evaporation rates (using solvents such as toluene or xylene). As an example, Figure 3 shows a comparison of the photoluminescence from films of pure TFB, pure F8BT and 1:1 blends of TFB:F8BT obtained both from toluene- and chloroform-based precursors.
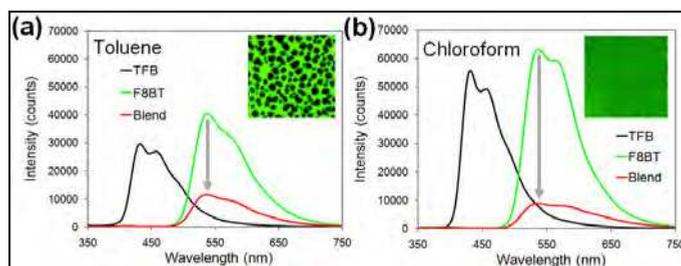

Fig. 3. Blended TFB-F8BT polyfluorene-based type-II heterostructures using different solvents. (a) Fluorescence emission from pure TFB, pure F8BT, and 1:1 ratio TFB:F8BT blended films obtained from toluene-based precursor solutions. (b) Same measurements obtained from chloroform-based precursors. The insets shows confocal fluorescence images of the domain structures in blended films. The insets are Adapted from (Moons, 2002) with permission.

In the toluene-based blend, the quenching of the F8BT emission by the TFB is much less pronounced compared with the chloroform-based blend. Indeed, the larger domains in the toluene-based blend provide more leasure for the photo-generated excitons to recombine radiatively before reaching another domain interface. In the chloroform-based blend, the probability for radiative-recombination is much lower since the photo-generated excitons are more likely to hit another domain interface and dissociate before they can recombine radiatively. This results precisely in the severely quenched F8BT fluorescence seen in Figure 3(b). Based on this result, it is obvious that larger domains will generally be preferable for light-emitting diode structures while smaller domains will be more desirable for photo-detector or photovoltaic device architectures.

For example, Figure 4 shows the optimal visible light-emitting diode architecture we obtain using a blended TFB:F8BT type-II heterostructure. Here, the structure is formed by spin-

coating a blended 1:1 toluene-based precursor atop a thin PEDOT:PSS hole-injection layer previously spin-coated directly on a commercial ITO substrate. After annealing at 160°C, the top electrode was evaporated through a shadow mask.
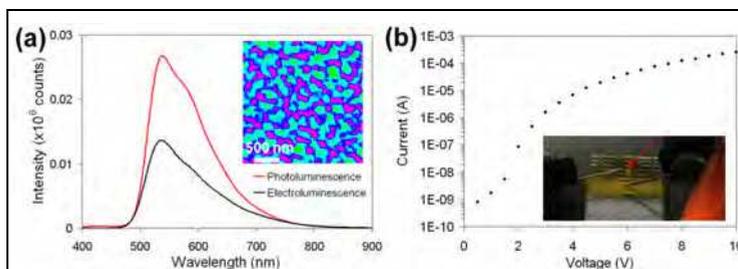

Fig. 4. Blended TFB-F8BT polyfluorene-based light-emitting diode. (a) Typical photoluminescence and electroluminescence from the TFB:F8BT blend at 19 V. The inset shows the typical domain structure obtained by phase separation between the hole-transporting TFB (pink) and the electron-transporting F8BT (green). (b) The current-voltage characteristics for this 520 nm LED structure. The inset shows a typical small-area device and the arrow points to the active device area.

3. Migrating the emission of polyfluorene-based LEDs towards the near infrared using lead-sulfosalt (PbS) colloidal quantum dots

Due to their relatively large HOMO-LUMO separations, conjugated polymer-based light-emitting diodes are perfectly suited for operation in the visible but their potential for near-infrared operation remains limited. As we mentioned previously, the hybrid integration of semiconductor nanocrystals and conjugated polymer material systems can provide an easy pathway for (1) improving the conjugated polymer-based devices' optoelectronic properties and/or (2) providing added functionality to the conjugated polymer-based device structures.

Indeed, semiconductor quantum dots have been recently used to controllably-alter the optoelectronic properties of a wide variety of host systems for biosensing, light-emitting or photovoltaic applications (Bakueva et al., 2003; Liu et al., 2009; McDonald et al., 2005; Steckel et al., 2003; X. Zhang et al., 2007).

Owing to low bandgaps, ultrafast recombination processes and large nonlinear coefficients, crystalline lead-salt chalcogenides (a sub-group of the IV-VI semiconductor family) have been one of the basic materials used in modern infrared light sources & lasers, photodetectors and high-performance thermoelectric for the last 50 years (Klann et al., 1995; Preier, 1979). Bulk lead sulfosalt (PbS) is well-suited for infrared optoelectronics, having a direct 0.41 eV bandgap and uncommonly large exciton binding energy (close to 300 meV).

Meanwhile, the first colloidal synthesis of chalcogenide semiconductor nanocrystals (CdS) in the mid-1980's (now referred-to as *colloidal quantum dots*) has provided a new pathway to producing low-cost optoelectronic materials with novel physical properties (Brus, 1984; Rossetti et al., 1983; Steigerwald et al., 1988). Then, it was only a matter of time before lead-salt nanocrystals were synthesized using the colloidal method (Hines & Scholes, 2003; I. Kang & Wise, 1997; Machol et al., 1993; Wang et al., 1987; Yang et al., 1996).

As shown in Figure 5, the TFB:F8BT conjugated polymer-based heterostructures also constitute an ideal host system for PbS semiconductor nanocrystals to provide low-cost and high-performance hybrid heterostructures for key applications such as lighting & displays, biomedical devices, lab-on-a-chip, flexible optoelectronics, night-vision and solar-energy harvesting device architectures.
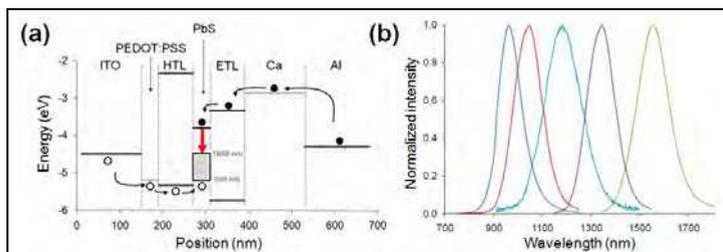

Fig. 5. Hybrid polyfluorene-based light-emitting heterostructures. (a) The TFB:F8BT system provides an ideal host system for PbS nanocrystal incorporation. (b) The incorporation of PbS nanocrystals can migrate their operation to the near-infrared (between 900 - 1600 nm), depending on the their size.

3.1 Colloidal synthesis of lead-sulfosalt nanocrystals with different shapes and sizes

Controlling the structural and optoelectronic properties of PbS nanostructures through improved hot-colloidal chemistry remains a very active field of research. As shown in Figure 6, the recent evolution of the early hot-colloidal lead-salt nanocrystal synthesis (Hines & Scholes, 2003) has lead to more complex nanostructures including nanorods & nanowires (Acharya et al., 2008; Dom et al., 2009; Ge et al., 2005; Yong et al., 2006; F. Zhang & Wong, 2009), star-shaped nanocrystals (Lee et al., 2002; Zhu et al., 2007), nanocubes (Zhao & Qi, 2006), octahedral nanocrystals (Cho et al., 2005; Koh et al., 2010) and core-shell nanocrystals (Petryga et al., 2008; Stouwdam et al., 2007; Swart et al., 2010; Warner & Cao, 2008). Most of these developments have occurred over the last five years.
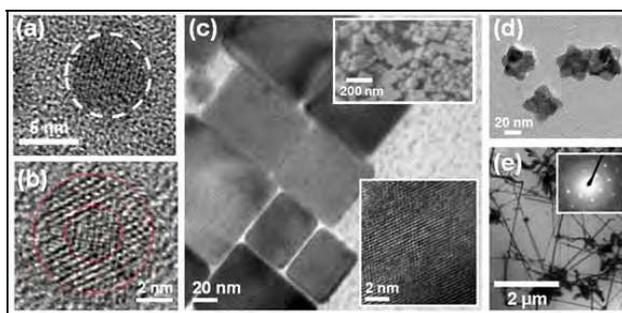

Fig. 6. Colloidal synthesis of exotic PbS nanostructures. (a) Typical PbS quantum dot, (b) PbS/CdS core-shell nanocrystal, (c) PbS nanocubes, (d) star-shaped PbS nanocrystals and (e) PbS nanowires, all synthesized in our lab using variations of the hot-colloidal method. The inset in (e) shows the selective area electron diffraction (SAED) used to confirm the single-crystal structure of the nanowires.

3.2 Directed self-assembly of lead-salt nanocrystals

More recently, the self-assembly of lead-salt nanocrystals into more complex nanowire (1D) (Cho et al., 2005; Jang et al., 2010; Koh et al., 2010), monolayer (2D) (Anikeeva et al., 2007, 2008; Coe-Sullivan et al., 2003; Konstantatos et al., 2005; Steckel et al., 2003; X. Zhang et al., 2007) and nanocrystalline films and superlattices structures (3D) (Hanrath et al., 2009; Klem et al., 2007, 2008; Luther et al., 2008; Talapin et al., 2005) with a wide range of most promising optoelectronic properties has rapidly become a very active field of research, largely due to its facile solution-based processing.
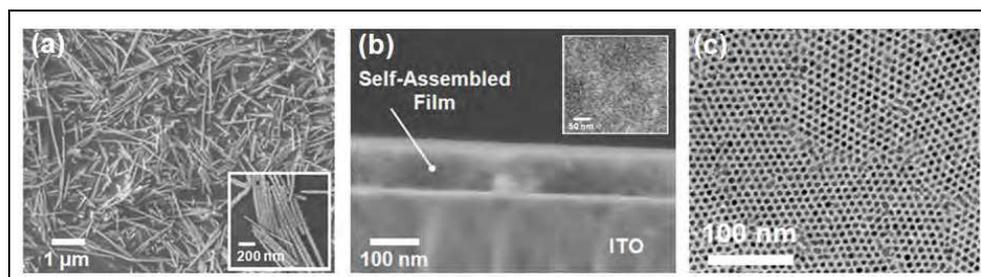

Fig. 7. (a) PbS nanowires formed by oriented-attachment of colloidal nanocrystals and (b) PbS nanocrystal films obtained by directed self-assembly. The inset shows the top-view of the self-assembled film. (c) This assembly process can be controlled down to reasonably-well organized monolayers.

Recently, exciting reports such as the observation of superb multiple-exciton generation efficiencies (Sargent, 2009; Sukhovatkin et al., 2009), highly-efficient hot-electron injection (Tisdale et al., 2010), and cold-exciton recycling (Klar et al., 2009), have propelled nanocrystalline lead-chalcogenide film structures to the forefront of cutting-edge research (M. S. Kang et al., 2009; W. Ma et al., 2009; Sambur et al., 2010; Steckel et al., 2003). Figure 7 shows typical examples of nanowires (1D), monolayers (2D) and films (3D) fabricated via the directed self-assembly of PbS nanocrystals synthesized by hot-colloidal method.

3.3 The incorporation of PbS nanocrystals in polymer-based host systems

Due to their band-structure alignment, we have shown that such PbS nanocrystals would be ideal for hybrid integration into the TFB:F8BT heterostructure to help migrate its operation towards the near-infrared. The most intuitively-obvious thing to do would be of course to simply mix colloidal quantum dots within the blended precursor prior to deposition. While this approach does work, threshold voltages and currents are generally very high, while quantum efficiencies and net output powers tend to be very low (Choudhury et al., 2010; Konstantatos et al., 2005). Indeed, this approach suffers from major fundamental drawbacks.

Assuming that the quantum dots are distributed homogeneously in the blended film, we also know that only the quantum dots located within tens of nanometers for the interfaces will be active. As such, this approach requires very large concentrations of quantum dots while most of them remain inactive. Moreover, it is likely that the incorporation of such large concentrations of quantum dots in the polymer host will have detrimental consequences on the performances of the polymer host itself.
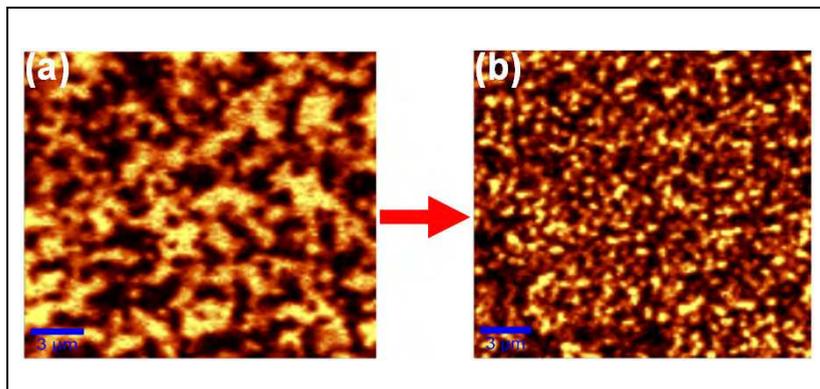
Fig. 8. The consequences of quantum-dot incorporation on blended polyfluorene-based film structures. Confocal fluorenscence mapping of the domain structure for the same toluene-blended TFB:F8BT (a) without PbS quantum dots and (b) impregnated with PbS quantum dots. The scale bars are 3 μm.

To verify the consequences of the PbS quantum dots incoporation, we used confocal fluorescence mapping of blended TFB:F8BT films with and without the colloidal quantum dots. The visible emission intensity maps (collected with a silicon detector) shown in Figure 8 reveal the domain structure for the blended films with and without quantum dots. There, the bright regions are F8BT-rich domains, while the dark regions represent TFB-rich domains. Without colloidal dots, Figure 8(a) shows significantly larger domains compared with the same blended film impregnated with near-infrared colloidal quantum dots (Fig. 8b).

Another factor to consider is the potential consequences of the nanoparticles incorporation on the crystalline phase of both polymers. Indeed, most polymers are known to consist of crystalline domains surrounded by amorphous chains. Indeed, the degree of crystallinity and the organization of those domains will also significantly impact the optoelectronic properties of the polyfluorenes (X. Ma et al., 2010). To study the consequences of nanoparticle incorporation on the structural organization of the polymers, we used electrospinning to pull polymer nanofibers (Sharma et al., 2010). Using a split collector during the electrospinning, it is possible to align those polymer fibers across the collector gap as shown in Figure 9(a). Using the 2D X-ray diffraction facility at the DND-CAT Synchrotron Research Center (AdvancedPhoton Source at the Argonne National Laboratory), we were able to observe the clear diffraction orders indicating that the crystallites in pure polymer fibers favor an alignment along the fibers such as shown in Figure 9(b). However, the incorporation of inert silica nanoparticles inside the polymer fibers disrupts this orientational ordering and yields a ring-like diffraction pattern shown in Figure 9(c), now suggesting a randomized polycrystalline structure such as shown in Figure 9(d). Indeed, by integrating for all azymuthal angles, we can confirm that the degree of crystallinity remains similar while the crystallites no longer show preferred alignment along the polymer fibers. This effect can also have very detrimental consequences of the optoelectronic properties of the polyfluorene-based device architectures incorporated with high concentrations of quantum dots.
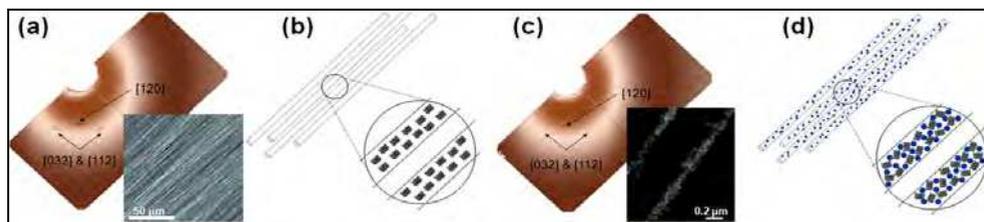
Fig. 9. (a) 2D X-ray diffraction pattern of pristine PEO polymer nanofibers (b) Schematic (not drawn to scale) showing oriented crystallite arrangement within the fibers. The white spaces between the polymer crystallites represent regions of amorphous polymer domains. (c,d) Results for PEO fibers incorporated with nanoparticles. Adapted from (Sharma et al., 2010) with permission. Copyright 2010 American Chemical Society.

3.4 The incorporation of PbS nanocrystals in polyfluorene-based bilayered type-II heterostructures

To alleviate those two fundamental problems, a better option explored more recently consists in depositing a thin self-assembled monolayer of quantum dots directly at the junction of the organic heterostructure between the hole- and electron-transporting organic materials (Steckel et al., 2003). However, this approach renders the whole fabrication sequence significantly more complex and usually involves the thermal evaporation of short-molecule organic semiconductors atop the quantum dots.

With long-molecule organics, this approach is even more delicate. One might suggest that simply spin-coating a pure F8BT layer atop a pure TFB layer or vice-versa would work. However, conjugated polymers from a same family tend to dissolve in similar solvents. As a consequence, the solvent of the second layer will significantly deteriorate the first layer. As shown in Figure 10, a viable approach to fabricating decent polyfluorene-based bilayered heterostructures consists in lifting-off a F8BT layer from one substrate and re-depositing directly on a TFB layer previously spin-coated on another substrate.
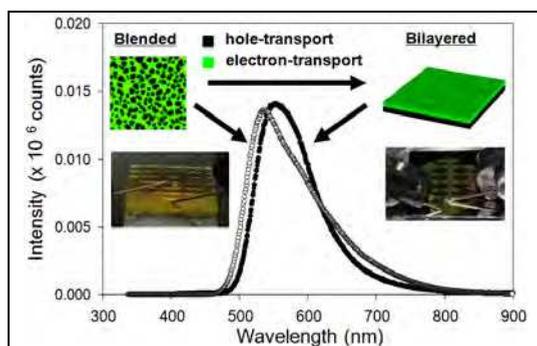

Fig. 10. Electroluminescence of blended (○) and bilayered (•) TFB-F8BT light-emitting diodes under 19V forward bias.

As shown in Figure 11, this approach can allow the incorporation of a thin monolayer of PbS quantum dots directly at the junction between the TFB and F8BT. Still, their performances

greatly suffer from poor injection efficiencies and from significant carrier losses into the organic layers (Konstantatos et al., 2005), most especially in the electron-transporting layer.
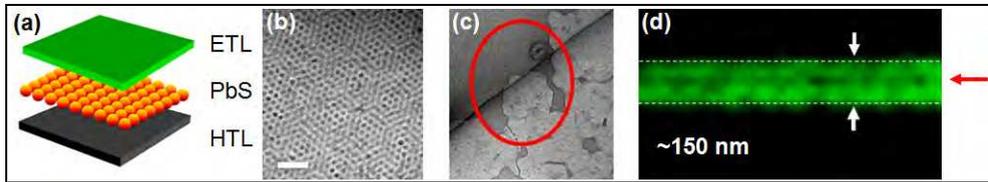

Fig. 11. Incorporation of PbS nanocrystals in polyfluorene-based bilayered type-II heterostructures. (a) Device schematics. (b) Self-assembled monolayer of PbS quantum dots. (c) Cross-sectional TEM of the structure after lift-off and deposition of the polymer layer atop the structure. (d) Cross-sectional confocal fluorescence intensity mapping showing the thin quantum-dot layer at the interface.

4. A new approach: The fabrication of high-performance hybrid polymer-nanocrystal heterostructures for near-infrared optoelectronics

As we have seen, PbS nanocrystals are typically synthesized using slightly modified versions of the widely-popular hot-colloidal method (Hines & Scholes, 2003). As such, the oleate capping group keeping colloidal nanocrystals stable in solution also severely limits charge transport between nanocrystals (S. Zhang et al., 2005). For this reason, previously-proposed near-infrared hybrid LED structures rely on colloidal quantum dots embedded within a polymer host matrix (Choudhury et al., 2010; Konstantatos et al., 2005), or use a monolayer of nanocrystals located directly at the junction of an organic heterostructure (Steckel et al., 2003). In both cases, we have seen that their performances greatly suffer from poor injection efficiencies and from significant carrier losses into the organic layers, thus providing output powers of a few micro-Watts (µW) at best (Konstantatos et al., 2005; X. Ma et al., 2010).

More recently, dithiol-based ligand exchange has been explored as a way of producing high-quality self-assembled PbS nanocrystalline film structures such as shown in Figure 12, with application in low-cost photovoltaic and photo-detector platforms (Klem et al., 2008). In this process, short dithiol linker molecules with strong thiolated bonds on both ends are used to exchange the long capping groups around colloidal nanocrystals, resulting in highly-conductive films of strongly-coupled cross-linked nanocrystals. As we will see, this breakthrough also provides new and exciting possibilities for novel near-infrared light-emitting device structures.

4.1 Conductivity and mobility of dithiol-treated nanocrystalline PbS film structures

For the first time, we investigated the optoelectronic properties of PbS nanocrystalline film structures cross-linked using carefully-controlled ethanedithiol (EDT) and benzenedithiol (BDT) ligand-exchange processes. To characterize the electronic properties of those self-assembled nanocrystalline film structures, we use two established methods. First, the charge extraction in linearly increasing voltage (CELIV) method described in Figure 13 can be used to measure both the conductivity and the majority carrier mobility. In view of the
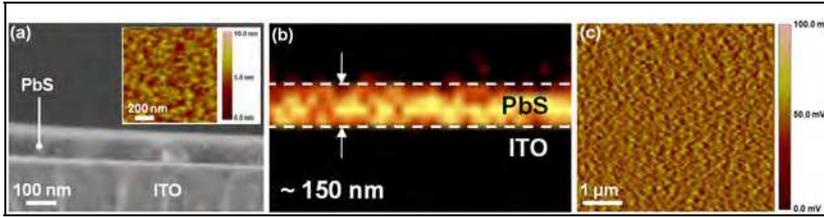
Fig. 12. Self-assembled PbS nanocrystalline film structure. (a) Cross-sectional SEM micrograph of a self-assembled film of PbS colloidal quantum dots formed by dithiol ligand-exchange chemistry. The inset shows a typical AFM mapping of the nanocrystalline PbS film surface revealing a 2 nm roughness parameter. (b) Cross-sectional map of the intensity of the 451 cm^{-1} Raman line associated with the 2LO-phonon vibration of the PbS film structure measured by confocal micro-Raman spectroscopy. (c) Conductive AFM (TUNA) mapping of the nanocrystalline film showing a good conductivity uniform across the surface.

p-type doping of the PbS nanocrystalline films, the CELIV measurement provides us with the hole-mobility for the dithiol-treated nanocrystalline films.

For CELIV measurements, the samples consist of a 250~350 nm-thick nanocrystalline films fabricated using the layer-by-layer spin coating method and sandwiched between ITO and Al contacts such as shown in Figure 13(a). As shown in Figure 13(b,c), a linearly-increasing bias is then applied across the sample while the transient currents are measured through the voltage drop across a 200 Ω load. The conductivity σ can then be obtained using (Juška et al., 2001):

$$\sigma = \frac{3}{2} \frac{d \Delta j}{t_{max} A} \tag{1}$$

while the hole mobility μ_h is calculated using (Juška et al., 2001):

$$\mu_h = \frac{2d^2}{3 A t_{max}^2 \left(1 + 0.36 \frac{\Delta j}{j_0} \right)} \tag{2}$$

The parameters t_{max}, j_0 and Δj in those equations can be obtained directly from the CELIV measurement, such as shown in Figure 13(b,c).

In contrast, the time-of-flight (TOF) method can be used to measure the minority carrier mobility. For TOF measurements, the samples have the same structure as for the CELIV measurements but require a much thicker nanocrystalline layer (1.0 ~ 1.5 μm) formed by depositing multiple layers of quantum dots. The 5 ns pulses of a Q-switched Nd:YAG laser are then used to excite the sample from the ITO side, while a reverse-bias is applied on the sample to extract the photo-generated minority carriers. In this case, the transient currents can also be recorded using the voltage drop across a 200 Ω load as shown in Figure 13(d). The electron mobility μ_e is then directly obtained as (Tiwari & Greenham, 2009):
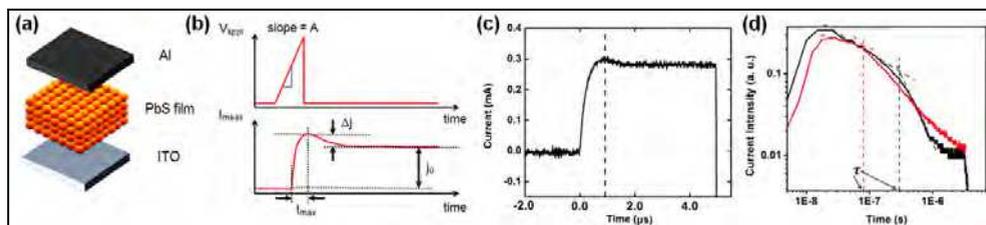
$$\mu_e = \frac{d^2}{V \tau} \tag{3}$$

Fig. 13. CELIV and TOF measurements of self-assembled PbS nanocrystalline film structure. (a) Device schematics. (b) For CELIV measurements, a linearly-increasing bias is applied across the sample while the transient currents are measured through the voltage drop across a 200 Ω load. (c) Typical CELIV transient current measured for an EDT-treated PbS film of thickness d= 250 nm using a linearly-increasing voltage with slope A = 400 KV/s. (d) TOF measured for EDT-treated nanocrystalline film structure with d = 1.2 μm under V = 15 V bias (black) and for BDT-treated nanocrystalline film structure with d = 1.1 μm under V = 27 V bias (red).

where d is the sample thickness, V the applied bias across the sample and τ is the transit time obtained from the TOF measurement such as shown in Figure 13(d).

The results of the conductivity, hole- and electron-mobility measurements for both EDT- and BDT-treated nanocrystalline film structures are summarized in Figure 14.
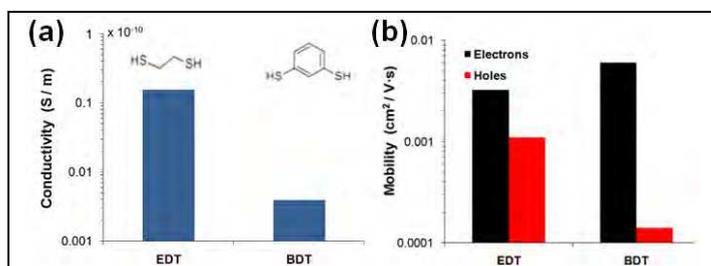

Fig. 14. Conductivity, hole- and electron-mobility measurements for EDT- and BDT-treated nanocrystalline film structures. (a) Conductivity measured using CELIV. (b) Electron-mobility measured using TOF (black) and hole-mobility measured using CELIV (red).

The smaller conductivity in the BDT-treated films simply suggests a significantly lower p-type doping concentration, most likely resulting from a better passivation of surface states compared with EDT. Moreover, the electron- and hole-mobilities are comparable for EDT-treated films. While we observe a modest increase in the electron mobility for the BDT-treated film despite using longer BDT molecules, it also leads to a significant drop in hole mobility. This is mostly because conjugated-dithiol molecular conductors (such as BDT) were previously shown not only to provide a physical linking between nanocrystals, but also a *conductive path* for electron transfer between nanocrystals through delocalization of the molecular electronic orbitals (Dadosh et al., 2005; Nitzan & Ratner, 2003). As such, the conjugated linker's LUMO and HOMO now provide additional energy barriers between nanocrystals for electrons and holes respectively. Since this energy barrier between nanocrystals is now significantly higher for holes compared with electrons, the carrier transport gets affected accordingly.

With BDT, the conjugation also provides substantial weight on the thiolated bonds that are directly coupled with the nanocrystals carriers wave-functions (Dadosh et al., 2005), thus directly increasing carrier transport for electrons. Indeed, previous experimental and theoretical models imply that the carrier transport through conjugated aryl dithiol molecules (such as BDT) occurs through the LUMO (electrons) level and not the HOMO (holes) (Nitzan & Ratner, 2003). This is consistent with both the increase of electron mobility and the large offset in electron and hole mobilities we observe for the BDT-treated nanocrystalline films.

4.2 Hybrid polymer-nanocrystal heterostructures for near-infrared optoelectronics

As we have seen with both the hybrid polymer-nanocrystal blends discussed in section 3.3 and the hybrid bilayered heterostructures discussed in section 3.4, their performances greatly suffer from poor injection efficiencies and from significant carrier losses into the organic layers (Choudhury et al., 2010; Konstantatos et al., 2005; Steckel et al., 2003). As we mentioned before, constraints on the electron-transporting material especially limit the overall performances of polymer-based optoelectronic devices (Moons, 2002).

As such, a new approach summarized in Figure 15 consists in substituting entirely the electron-transporting organic material, with a self-assembled film of cross-linked PbS nanocrystals deposited atop a hole-transporting polymer film structure. As shown in Figure 15(c), this new hybrid polymer-nanocrystal architecture allows direct electron injection without any additional injection layer and provides significantly better electron transport, thus leading to highly-improved LED devices.
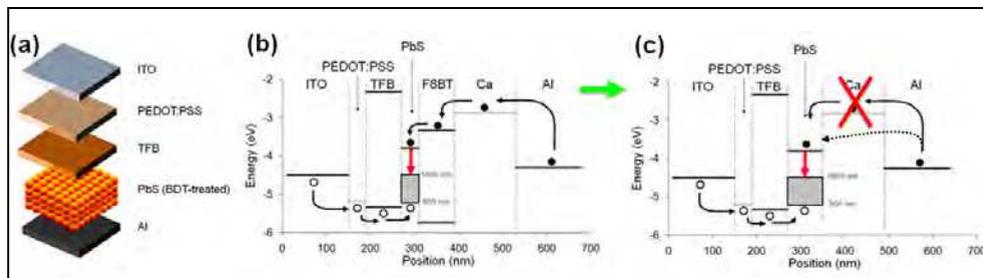

Fig. 15. Novel hybrid polymer-nanocrystal heterostructures for near-infrared LEDs. (a) Device schematics. (b) Energy diagram of the previously studied near-IR LED structures using nanocrystals embedded within a polymer host matrix, or a monolayer of quantum dots introduced at the junction of the organic heterostructure in-between the hole- and electron-transporting organic materials. (c) Energy diagram of the proposed near-IR LED architecture replacing the electron-transporting organic layer, with a self-assembled film of cross-linked PbS nanocrystals deposited atop a hole-transporting polymer film structure.

4.3 High-performance near-infrared LEDs using hybrid polymer-nanocrystal heterostructures

As shown in Figure 16, high-performance near-IR LEDs can be fabricated at extremely low cost using a very simple all solution-based processing approach.

To fabricate those structures, the ITO substrate is first patterned using standard photolithography and wet-etching processes before spin-coating of a very thin 30 nm-thick layer of PEDOT:PSS. As we mentioned before, this thin layer of PEDOT:PSS plays the dual role of facilitating the hole-injection while alleviating the detrimental effects of the surface roughness of the ITO film on the structural properties of the hole-transporting polymer. A toluene-based TFB solution is then spin-coated to provide a 120 nm-thick TFB film atop the PEDOT:PSS. Since the PEDOT:PSS is immune to toluene, there is no solvent-compatibility issues. Then, a solution of PbS quantum dots suspended in hexane is spin-coated atop the TFB, prior to performing the ligand-exchange process using the dithiol molecule diluted in acetonitrile. While the PEDOT:PSS would be affected by both the hexane and acetonitrile solutions, the TFB provides an efficient protection barrier for both solvents, thus preserving the structural integrity of the whole structure.
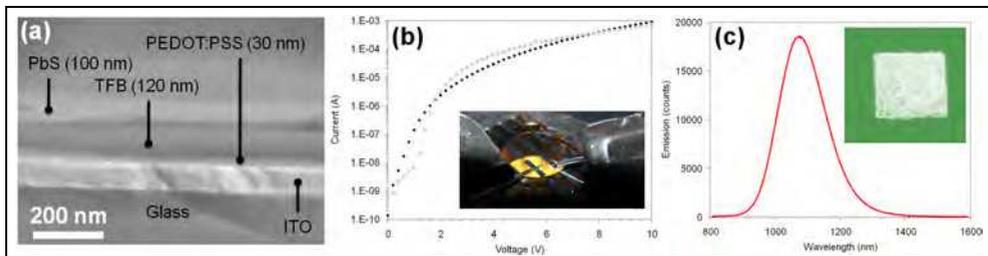

Fig. 16. High-Performance near-infrared LEDs using all solution-based processing. (a) Cross-sectional SEM micrograph showing the optimized structure of the device. (b) Device current-voltage characteristics for hybrid LED structure (•) and a polymer-only control device (◦). The inset shows the actual device atop the entry port of an integrating sphere while the near-IR electroluminescence is collected through the transparent substrate. (c) Emission spectra of a typical 1050 nm LED. The inset image shows the actual near-IR emission of a 1 mm² device measured using a near-IR camera coupled to a 2X objective.

As shown in Figure 16(b), the polymer-only control device reaches a clear single-carrier (hole) trap-limited regime around 1 Volt, before reaching a space-charge limited operation regime around 2 Volts. This is consistent with the large energy barrier at the TFB-aluminum interface. For the LED device with the BDT-treated nanocrytalline film structure, measurements indicate a much higher current density at low voltages originating from the efficient electron-injection at the metal-PbS interface. Here, the lower slope in the trap-limited region simply suggests different transport and trapping mechanisms in the nanocrystalline film compared with the TFB. These highly-efficient LED structures can operate anywhere between 1000 and 1600 nm depending on the nanocrystals used while providing external quantum efficiencies as high as 0.7% and ouput powers close to 80 μW.

While the conventional ethanedithiol (EDT)-based ligand-exchange treatment is known to work well for photovoltaic structures (Luther et al., 2008), it yields only relatively poor LED structures compared to the phenomenal results achieved using benzendithiol (BDT)-based treatment. This disparity can be readily explained now based on the conductivity and mobility results presented in Figure 14. Indeed, the EDT treatement provides higher conductivities due to higher p-type doping and comparable electron- and hole- mobilities. As such, both the hole current and nonradiative Auger recombination will be orders of

magnitude larger than for BDT-treated films. Moreover, the large hole-current would for EDT-treated films would ideally require a hole-barrier at the metal-nanocrystal interface. While we tried to use a TiO_2 barrier to reduce the hole-current for such films, we observed that this barrier significantly impedes the electron injection.

With the BDT-treatment, the hole-mobility drops significantly. As such, there is no need to have a hole-blocking barrier at the metal-PbS interface since the holes don't make it to this interface anyway. Even better, this dramatic reduction in hole mobility is associated with a modest increase in electron mobility. As we know, everything happens at the junction of this hybrid polymer-nanocrystal heterostructure. Using the BDT-treated nanocrystalline films, electrons can be very efficiently injected from one side and holes from the other. Moreover, the hole-transporting polymer bilayer provides an efficient electron barrier while the BDT-treatment provides a good mobility-barrier for holes in the nanocrystalline film. As such, the carriers are efficiently delivered and confined close to the junction (active region). Due to the low hole-mobility, the excitons then bind and stay close to the junction, having plenty of time to recombine radiatively while avoiding metal quenching from the metal-PbS interface.

5. Conclusion

While π-conjugated polymer-based light-emitting diodes are perfectly suited for the visible, their potential for near-infrared operation remains limited. However, the hybrid integration of semiconductor nanocrystals and conjugated polymer material systems can provide an easy pathway for (1) improving the conjugated polymer-based devices optoelectronic properties and/or (2) providing added functionality to the conjugated polymer-based device structures. Because the oleate capping groups keeping colloidal lead-chalcogenide nanocrystals stable also inhibit carrier transport, previously-proposed hybrid near-infrared LED structures usually rely on nanocrystals embedded within a polymer host matrix, or use a self-assembled monolayer of colloidal quantum dots located at the junction of an organic heterostructure directly between hole- and electron-transporting organics. We have demonstrated why both these hybrid polymer-nanocrystal blends and the hybrid bilayered heterostructures greatly suffer from poor injection efficiencies and from significant carrier losses into the organic layers, while limited electron-transporting materials especially limit the overall performances of those polymer-based optoelectronic devices.

Here, we report an all solution-based method producing efficient hybrid polymer-nanocrystal multilayered heterostructures for light-emission in the near-infrared (1050-1600 nm). After optimization device structure, we obtain low-cost near-infrared light-emitting diodes with external quantum efficiency (EQE) as high as 0.7% and up to 80 µW output from devices entirely processed in ambient air and with no encapsulation. This approach relies on a carefully-controlled layer-by-layer benzenedithiol (BDT) ligand-exchange to achieve direct charge injection and better transport. In comparison with this BDT treatment, the conventional ethanedithiol (EDT)-based treatment provides poor LED structures. As we show, the high performances of our devices can be explained by the different doping levels and electron & hole mobilities resulting from the BDT versus EDT treatments.

In the future, this easy, robust, low-temperature and substrate-independent approach has the potential to become extremely useful for flexible and/or reconfigurable integrated opto-

electronic platforms, biological imaging & sensing, lab-on-a-chip and thermoelectronic platforms. Moreover, this method could also be extended to other colloidal nanocrystals such as PbSe (for longer wavelengths) or CdSe (for the visible). Finally, the large refractive index of these self-assembled nanocrystalline film structures offers the possibility of incorporating these electroluminescent structures directly onto silicon substrates to work as light source or in more complex optoelectronic device architectures.

6. Acknowledgment

7. References

Acharya, S., Gautam, U. K., Sasaki, T., Bando, Y., Golan, Y., & Ariga, K., Ultra Narrow PbS Nanorods with Intense Fluorescence, *Journal of the American Chemical Society*, Vol.130 (2008), pp. 4594-4595

Anikeeva, P. O., Halpert, J. E., Bawendi, M. G., & Bulovic, V., Electroluminescence from a Mixed Red-Green-Blue Colloidal Quantum Dot Monolayer, *Nano Letters*, Vol.7 (2007), pp. 2196-2200

Anikeeva, P. O., Madigan, C. F., Halpert, J. E., Bawendi M. G., & Bulovic, V., Electronic and excitonic processes in light-emitting devices based on organic materials and colloidal quantum dots, *Physical Review B*, Vol.78 (2008), pp. 085434-8

Arias, A. C. MacKenzie, J. D., Stevenson, R., Halls, J. J. M., Inbasekaran, M., Woo, E. P., Richards, D., & Friend, R. H., Photovoltaic Performance and Morphology of Polyfluorene Blends: A Combined Microscopic and Photovoltaic Investigation, *Macromolecules*, Vol.34 (2001), pp. 6005-6013

Bakueva, L., Musikhin, S., Hines, M. A., Chang, T.-W. F., Tzolov, M., Scholes, G. D., & Sargent, E. H., Size-tunable infrared (1000-1600 nm) electroluminescence from PbS quantum-dot nanocrystals in a semiconducting polymer, *Applied Physics Letters*, Vol.82 (2003), pp. 2895-2897

Brus, L. E., Electron-electron and electron-hole interactions in small semiconductor crystallites: The size dependence of the lowest excited electronic state, *Journal of Chemical Physics*, Vol.80 (1984), pp. 4403-4409

Cho, K.-S., Talapin, D. V., Gaschler, W., & Murray, C. B., Designing PbSe Nanowires and Nanorings through Oriented Attachment of Nanoparticles, *Journal of the American Chemical Society*, Vol.127 (2005), pp. 7140-7147

Choudhury, K. R., Song, D. W., & So, F., Efficient solution-processed hybrid polymer–nanocrystal near infrared light-emitting devices. *Organic Electronics*, Vol.11 (2010), pp. 23-28

Coe-Sullivan, S., Woo, W.-K., Steckel, J. S., Bawendi, M., & Bulovic, V., Tuning the performance of hybrid organic/inorganic quantum dot light-emitting devices, *Organic Electronics*, Vol.4 (2003), pp. 123-130

Dadosh, T., Gordin, Y., Krahne, R., Khivrich, I., Mahalu, D., Frydman, V., Sperling, J., Yacoby, A., & Bar-Joseph, I., Measurement of the conductance of single conjugated molecules, *Nature*, Vol.436 (2005), pp. 677-680

Dom, A., Wong C. R. & Bawendi, M. G., Electrically Controlled Catalytic Nanowire Growth from Solution, *Advanced Materials*, Vol.21 (2009), pp. 3479-3482

Ge, J.-P., Wang, J., Zhang, H.-X., Wang, X., Peng, Q., & Li, Y.-D., Orthogonal PbS Nanowire Arrays and Networks and Their Raman Scattering Behavior, *Chemistry - A European Journal*, Vol.11 (2005), pp. 1889-1894

Hanrath, T., Choi, J. J. & Smilgies,D.-M., Structure/Processing Relationships of Highly Ordered Lead Salt Nanocrystal Superlattices, *ACS Nano*, Vol.10 (2009), pp. 2975-2988

Hines, M. A., & Scholes, G. D., Colloidal PbS Nanocrystals with Size-Tunable Near-Infrared Emission: Observation of Post-Synthesis Self-Narrowing of the Particle Size Distribution, *Advanced Materials*, Vol.15 (2003), pp. 1844-1849

Jang, S. Y., Song, Y. M., Kim, H. S., Cho, Y. J., Seo, Y. S., Jung, G. B., Lee, C.-W., Park, J., Jung, M., Kim, J., Kim, B., Kim, J.-G., & Kim, Y.-J., Three Synthetic Routes to Single-Crystalline PbS Nanowires with Controlled Growth Direction and Their Electrical Transport Properties, *ACS Nano*, Vol.4 (2010), pp. 2391-2401

Juška, G., Viliūnas, M., Arlauskas, K., Nekrašas, N., Wyrsch, N., & Feitknecht, L., Hole drift mobility in μc-Si:H, *Journal of Applied Physics*, Vol.89 (2001), pp. 4971-4977

Kang I. &Wise, F. W., Electronic structure and optical properties of PbS and PbSe quantum dots, *Journal of the Optical Society of America B*, Vol.14 (1997), pp. 1632-1646

Kang, M. S., Lee, J., Norris, D. J., & Frisbie, C. D., High carrier densities achieved at low voltages in ambipolar PbSe nanocrystal thin-film transistors, *Nano Letters*, Vol.9 (2009), pp. 3848-3852

Klann, R. H., Hofer, T., Thomas Buhleier, R. E., & Thomas Tomm, J. W., Fast recombination processes in lead chalcogenide semiconductors studied via transient optical nonlinearities, *Journal of Applied Physics,* Vol.77 (1995), pp. 277-286

Klar, T. A., Franzl, T., Rogach, A. L., & Feldmann, J., Super-efficient exciton tunneling in layer-by-layer semiconductor nanocrystal structures, *Advanced Materials,* Vol.17 (2009), pp. 769-773

Klem, E. J. D., MacNeil, D. D., Cyr, P. W., Levina, L., & E. H. Sargent, E. H., Efficient solution-processed infrared photovoltaic cells: Planarized all-inorganic bulk heterojunction devices via inter-quantum-dot bridging during growth from solution, *Applied Physics Letters*, Vol.90 (2007), pp. 183113-3

Klem, E. J. D., Shukla, H., Hinds, S., MacNeil, D. D., Levina, L., & Sargent, E. H., Impact of dithiol treatment and air annealing on the conductivity, mobility, and hole density in PbS colloidal quantum dot solids, *Applied Physics Letters*, Vol.92 (2008), pp. 212105-3

Koh, W.-K., Bartnik, A. C., Wise F. W., & Murray, C. B., Synthesis of Monodisperse PbSe Nanorods: A Case for Oriented Attachment, *Journal of the American Chemical Society*, Vol.132 (2010), pp. 3909-3913

Konstantatos, G., Huang, C., Levina, L., Lu, Z., & Sargent, E. H., Efficient Infrared Electroluminescent Devices Using Solution-Processed Colloidal Quantum Dots, *Advanced Functional Materials*, Vol.15 (2005), pp. 1865-1869

Lee, S.-M., Jun, Y.-W., Cho, S.-N., & Cheon, J., Single-Crystalline Star-Shaped Nanocrystals and Their Evolution: Programming the Geometry of Nano-Building Blocks, *Journal of the American Chemical Society*, Vol.124 (2002), pp. 11244-11245

Liu, J., Wang, S., Bian, Z., Shan M., & Huang, C., Organic/inorganic hybrid solar cells with vertically oriented ZnO nanowires, *Applied Physics Letters*, Vol.94 (2009), pp. 173107-3

Luther, J. M., Law, M., Song, Q., Perkins, C. L., Beard, M. C., & Nozik, A. J., Structural, Optical, and Electrical Properties of Self-Assembled Films of PbSe Nanocrystals Treated with 1,2-Ethanedithiol, *ACS Nano*, Vol.2 (2008), pp. 271-280

Ma, W., Luther, J. M., Zheng, H., Wu, Y., & Alivisatos, A. P., Photovoltaic devices employing ternary PbS_xSe_{1-x} nanocrystals, *Nano Letters*, Vol.9 (2009), pp. 1699-1703

Ma, X., Xu F., & Cloutier, S. G., High-Performance 1550 nm Polymer-Based LEDs on Silicon using Hybrid Polyfluorene-Based Type-II Heterojunctions, *Proceedings fo the 7th Inter. Conference on Group-IV Photonics*, Beijing, China, October 2010

Machol, J. L., Wise, F. W., Patel, R. C., & Tanner, D. B., Vibronic quantum beats in PbS microcrystallites, *Physical Review B*, Vol.48 (1993), pp. 2819-2822

MacDiarmid, A. G., Synthetic metals: a novel role for organic polymers, *Current Applied Physics*, Vol.1 (2001), pp. 269-317

McDonald, S. A., Konstantatos, G., Zhang, S., Cyr, P. W., Klem, E. J. D., Levina L., & Sargent, E. H., Solution-processed PbS quantum dot infrared photodetectors and photovoltaics, *Nature Materials*, Vol.4 (2005), pp. 138-142

McNeill, C. R., Watts, B., Thomsen, L., Belcher, W. J., Greenham, N. C., Dastoor, P. C., & Ade, H., Evolution of Laterally Phase-Separated Polyfluorene Blend Morphology Studied by X-ray Spectromicroscopy, *Macromolecules,* Vol.42 (2009), pp. 3347-3352

Moons, E., Conjugated polymer blends: linking film morphology to performance of light emitting diodes and photodiodes, Journal of Physics: Condensed Matter*,* Vol.14 (2002), pp. 12235-12252

Morteani, A. C., Dhoot, A. S., Kim, J.-S., Silva, C., Greenham, N. C., Murphy, C., Moons, E., Cina, S., Burroughes, J. H., & Friend, R. H., Barrier-Free Electron-Hole Capture in Polymer Blend Heterojunction Light-Emitting Diodes, *Advanced Materials,* Vol.15 (2003), pp. 1708-1715

Nitzan, A., & Ratner, M. A., Electron transport in molecular wire junctions, *Science*, Vol.300 (2003), pp. 1384-1389

Pietryga, J. M., Werder, D. J., Williams, D. J., Casson, J. L., Schaller, R. D., Klimov, V. I., & Hollingsworth, J. A., Utilizing the Lability of Lead Selenide to Produce Heterostructured Nanocrystals with Bright, Stable Infrared Emission, *Journal of the American Chemical Society,* Vol.130 (2008), pp. 4879-4885

Preier, H., Recent Advances in Lead-Chalcogenide Diode Lasers, *Applied Physics,* Vol.20 (1979), pp. 189-206

Rossetti, R., Nakahara, S., & Brus, L. E., Quantum size effects in the redox potentials, resonance Raman spectra, and electronic spectra of CdS crystallites in aqueous solution, *Journal of Chemical Physics,* Vol.79 (1983), pp. 1086-1088

Sambur, J. B., Novet, T., & Parkinson, B. A., Multiple exciton collection in a sensitized photovoltaic system, *Science,* Vol.330 (2010), pp. 63-66

Sargent, E. H., Infrared photovoltaics made by solution processing, *Nature Photonics*, Vol.3 (2009), pp. 325-331

Sharma, N., McKeown, S. J., Ma, X., Pochan, D. J., & Cloutier, S. G., Structure-Property Correlations in Hybrid Polymer-Nanoparticle Electrospun Fibers and Plasmonic Control over their Dichroic Behavior, *ACS Nano*, Vol.4 (2010), pp. 5551-5555

Steckel, J. S., Coe-Sullivan, S., Bulović, V., & Bawendi, M. G., 1.3 µm to 1.55 µm Tunable Electroluminescence from PbSe Quantum Dots Embedded within an Organic Device, *Advanced Materials*, Vol.15 (2003), pp. 1862-1866

Steigerwald, M. L., Alivisatos, A. P., Gibson, J. M., Harris, T. D., Kortan, R., Muller, A. J., Thayer, A. M., Duncan, T. M., Douglas, D. C., & Brus, L. E., Surface Derivatization and Isolation of Semiconductor Cluster Molecules, *Journal of the American Chemical Society*, Vol.110 (1988), pp. 3046-3050

Stouwdam, J. W., Shan, J., van Veggel, F. C. J. M., Pattantyus-Abraham, A. C., Young J. F., & Raudsepp, M., Photostability of Colloidal PbSe and PbSe/PbS Core/Shell Nanocrystals in Solution and in the Solid State, *Journal of Physical Chemistry C*, Vol.111 (2007), pp. 1086-1092

Sukhovatkin, V., Hinds, S., Brzozowski, L., & Sargent, E. H., Colloidal quantum-Dot photodetectors exploiting multiexciton generation, *Science*, Vol.324 (2009), pp. 1542-1544

Swart, I., Sun, Z., Vanmaekelbergh D., Liljeroth, P., Hole-Induced Electron Transport through Core-Shell Quantum Dots: A Direct Measurement of the Electron-Hole Interaction, *Nano Letters*, Vol.10 (2010), pp. 1931-1935

Talapin, D. V., & Murray, C. B., PbSe Nanocrystal Solids for n- and p-Channel Thin Film Field-Effect Transistors, *Science*, Vol.310 (2005), pp. 86-91

Tisdale, W. A., Williams, K. J., Timp, B. A., Norris, D. J., Aydil, E. S., & Zhu, X.-Y., Hot-electron transfer from semiconductor nanocrystals, *Science*, Vol.328 (2010), pp. 1543-1547

Tiwari, S., & Greenham, N. C., Charge mobility measurement techniques in organic semiconductors, *Opt. Quant. Electron.*, Vol.41 (2009), pp. 69-89

Warner J. H., & Cao, H., Shape control of PbS nanocrystals using multiple surfactants, *Nanotechnology*, Vol.19 (2008), pp. 305605-5

Wang, Y., Suna, A., Mahler, W., & Kasowski, R., PbS in polymers: From molecules to bulk solids, *Journal of Chemical Physics*, Vol.87 (1987), pp. 7315-7322

Yang, J. P., Qadri, S. B., & Ratna, B. R., Structural and Morphological Characterization of PbS Nanocrystallites Synthesized in the Bicontinuous Cubic Phase of Lipid, *Journal of Physical Chemistry*, Vol.100 (1996), pp. 17255-17259

Yong, K.-T., Sahoo, Y., Choudhury, K. R., Swihart, M. T., Minter, J. R., & Prasad, P. N., Control of the Morphology and Size of PbS Nanowires Using Gold Nanoparticles, *Chemistry of Materials*, Vol.18 (2006), pp. 5965-5972

Zhang, F., & Wong, S. S., Controlled Synthesis of Semiconducting Metal Sulfide Nanowires, *Chemistry of Materials*, Vol.21 (2009), pp. 4541-4554

Zhang S., Cyr, P. W., McDonald, S. A., Konstantos, G., & Sargent, E. H., Enhanced infrared photovoltaic efficiency in PbS nanocrystal/semiconducting polymer composites:

600-fold increase in maximum power output via control of the ligand barrier, *Applied Physics Letters*, Vol.87 (2005), pp. 233101-3

Zhang, X., Dong, X., Liu, Y., Kai, G., Wang, Z., Li, L., Han X., & Li, Y., Near-infrared emission from PbS Quantom Dots in polymer matrix, *Optoelectronics Letters*, Vol.3 (2007), pp. 337-342

Zhao, N., & Qi, L., Low-Temperature Synthesis of Star-Shaped PbS Nanocrystals in Aqueous Solutions of Mixed Cationic/Anionic Surfactants, *Advanced Materials*, Vol.18 (2006), pp. 359-362

Zhu, J., Peng, H., Chan, C. K., Jarausch, K., Zhang, X. F., & Cui, Y., Hyperbranched Lead Selenide Nanowire Networks, *Nano Letters*, Vol.7 (2007), pp. 1095-1099
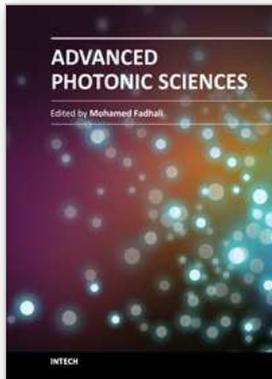
Advanced Photonic Sciences

Edited by Dr. Mohamed Fadhali

The new emerging field of photonics has significantly attracted the interest of many societies, professionals and researchers around the world. The great importance of this field is due to its applicability and possible utilization in almost all scientific and industrial areas. This book presents some advanced research topics in photonics. It consists of 16 chapters organized into three sections: Integrated Photonics, Photonic Materials and Photonic Applications. It can be said that this book is a good contribution for paving the way for further innovations in photonic technology. The chapters have been written and reviewed by well-experienced researchers in their fields. In their contributions they demonstrated the most profound knowledge and expertise for interested individuals in this expanding field. The book will be a good reference for experienced professionals, academics and researchers as well as young researchers only starting their carrier in this field.

How to reference

In order to correctly reference this scholarly work, feel free to copy and paste the following:

Sylvain G. Cloutier (2012). Hybrid Polyfluorene-Based Optoelectronic Devices, Advanced Photonic Sciences, Dr. Mohamed Fadhali (Ed.), ISBN: 978-953-51-0153-6, InTech, Available from: http://www.intechopen.com/books/advanced-photonic-sciences/hybrid-polyfluorene-based-optoelectronic-devices

INTECH
open science | open minds